Japanese Journal of Applied Physics
Vol. 47, No. 10, 2008, pp. 8113–8119

©2008 The Japan Society of Applied Physics

Pulsed Laser-Induced Rapid Surface Cooling and Amorphization

Longzhang TIAN and Xinwei WANG[1]*

Department of Mechanical Engineering, The University of Nebraska-Lincoln, Lincoln, NE 68588-0656, U.S.A.
[1]*Department of Mechanical Engineering, 3027 H.M. Black Engineering Building, Iowa State University, Ames, IA 50011-2161, U.S.A.*

(Received April 12, 2008; accepted July 23, 2008; published online October 17, 2008)

In this work, hybrid atomistic-macroscale simulation is conducted to explore the crystallization and amorphization of Si surface in the situation of fast melting and solidification induced by ultrafast laser heating and heat conduction. Our work is focused on investigating the relationship between the amorphization threshold (E_c) and the laser pulse width (t_g). An empirical correlation $E_c = 448.76 \times t_g{}^{0.56}$ is obtained to relate the critical fluence to the laser pulse width. By exploring the microstructure of the amorphous and crystalline state of Si, a sharp interface of about 0.6 nm thickness is observed between the amorphous layer and the crystalline Si. The relationship between the final thickness of amorphous layer and the fluence of the laser pulse is further studied in this work. Employing laser pulses with full width at half maximum (FWHM) equal to 6.67 ns, the formation and recrystallization processes of a 12-nm-thick amorphous layer is investigated.
[DOI: 10.1143/JJAP.47.8113]

KEYWORDS: Si amorphization, ultrathin film, pulsed laser, ultrafast conduction cooling

1. Introduction

Pulsed-laser annealing techniques are widely used in the fabrication of amorphous semiconductors, which have various applications in solar cells, xerography, and flat-panel displays.[1–6] Laser-induced crystallization and amorphization of Si films, one of the most interesting areas of amorphous semiconductors, has great potential applications in the fabrication of thin film transistors (TFTs) for high-definition active matrix liquid crystal displays (AMLCDs) and the nano-imprinting technique for the fabrication of photonic bandgap crystals (PBCs).[6–8] Due to the rapid heating by pulsed lasers, a significant temperature gradient will be established in the solid region adjacent to the molten part, which could lead to ultrafast cooling. As a result, the Si will feature new melting and solidification characteristics, and an ultrathin amorphous Si (a-Si) layer could form.

To understand the microscopics of melting and solidification processes induced by the pulsed laser, much research in numerical simulation and experiments has been done in this field. Using a 30-ns-XeCl excimer laser, Sameshima and Usui explored the role of film thickness and recalescence caused by latent heat for amorphization of Si films on quartz substrate. They found that Si films were completely amorphized for films thinner than 18 nm.[9] Using 2.5 or 0.7 ns laser pulses, Cullis *et al.* demonstrated that the maximum growth velocities of the principal low index Si surfaces lie in the order of (001) > (011) > (112) > (111).[10] When the crystal growing rate is beyond the maximum velocity, the crystal growth breaks down and a final amorphous solid phase is produced. This order of growth velocities in different orientations was also predicted by molecular dynamics (MD) simulations conducted by Landman *et al.*[11] The accrual amorphization threshold of interface velocity has been measured by transient conductivity experiments and shown to be 15.8 m/s for (001) Si and 14.6 m/s for (111) Si.[12–14] Above these critical velocities, amorphization occurs. The process of excimer-laser crystallization of a-Si films was also investigated by Munetoh *et al.* using MD simulations and by Ishihara *et al.* using the transmission electron microscopy (TEM) and time-resolved optical reflectivity (TROR) spectroscopy.[15,16]

During the crystallization and amorphization of Si, the rapid cooling rate is usually caused by the pulsed laser. However, the MD simulations done in this area mostly focused on the crystallization process of liquid Si. In these simulations, an initial equilibrium state of Si at high temperatures was usually used and the solidification was driven by a constant cooling. This did not provide the relationship between the laser properties, such as fluence and pulse width, and the crystal structure of Si after melting and solidification. Nor did their work study the solidification process under the actual cooling rate caused by heat conduction through the solid Si substrate.

In this work, hybrid atomistic-macroscale modeling is conducted to explore the solidification/crystallization characteristics of (001) Si under ultrafast laser heating and natural cooling situation. MD simulations using the environment-dependent interatomic potential (EDIP) is combined with the finite difference (FD) method to capture the structure change during laser heating and post-laser solidification considering the long-time heat conduction in the solid domain. The evolution of sample structures is characterized using crystallinity function and radial distribution function to illuminate phase changes during laser heating and natural cooling process. The final crystal structure of samples after laser heating is also investigated. For different laser pulse widths, the critical fluences are calculated above which the post-laser solidification/cooling will result in an amorphous layer. The thickness of the amorphous layer created by laser heating with different laser fluences and the recrystallization process of the amorphous layer heated by a second laser pulse are explored as well.

2. Methodologies of Simulation

2.1 Computational domain construction

The potential used for MD simulation of Si is the EDIP which was developed by Justo *et al.* and Bazant *et al.* for bulk Si.[17,18] This potential contains two- and three-body interactions with theoretically motivated functional forms and provides a much realistic prediction in simulating

*E-mail address: xwang3@iastate.edu

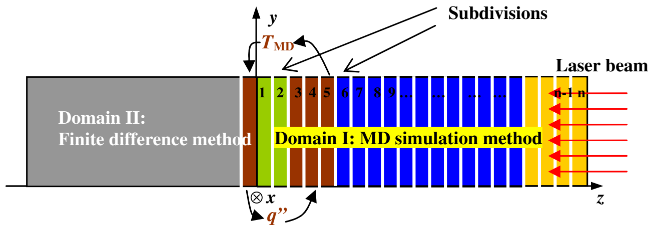

Fig. 1. (Color online) Schematic of the computational domain. Domain I ($z > 0$) is modeled by MD simulation. The green region is kept still to prevent Domain I from moving under the laser irradiation; the blue region is the target; the red region is used to calculate the boundary temperature and heat flux for MD and FD simulation coupling; and the yellow region is the additional empty computational region. Domain II ($z < 0$) is simulated using the FD method to provide the actual cooling rate caused by heat conduction.

quenching directly from the liquid to amorphous phase of Si. While giving more accurate prediction, the EDIP possesses the same level of efficiency as the popular Stillinger–Weber potential and makes it feasible to conduct MD simulation for systems with a large number of atoms.[19]

According to the optical absorption and melting depth of Si for the lasers used in this work,[20] the whole physical space is divided into two domains: the Si thin film and Si substrate or the molten region and the solid part for bulk Si. Figure 1 illustrates the design of the computational domain for hybrid atomistic-macroscale modeling. Materials in Domain I is subjected to picosecond (ps) and nanosecond (ns) laser heating and experience intense structural change. MD simulation is conducted to model the material behavior in Domain I. Materials in Domain II experiences heat conduction. Therefore, the FD method is used to model the heat transfer in Domain II. The one-dimensional heat conduction equation is solved in Domain II for heat transfer. The thermophysical properties (specific heat and thermal conductivity) of the material are temperature dependent and updated in the FD simulation every time step. Periodical boundary conditions are used along the x and y directions and free boundary conditions are used in the z direction shown in Fig. 1.

As shown in Fig. 1, Domain I is divided into thin layers according to the cutoff distance of the EDIP.[17] To prevent Domain I from moving along the negative z direction, two layers (green region in Fig. 1) in which atoms are kept still are added to the left of Domain I. Empty layers (yellow region in Fig. 1) are added to the right end of Domain I to allow volume increase and vaporization during laser heating. For thermal boundary coupling between Domains I and II, the temperature calculated at the backside of Domain I (left three layers, dark red region in Fig. 1) is used as the right boundary condition for Domain II. It is shown in our simulation this boundary temperature has a strong oscillation with time due to statistical uncertainties in MD simulation. Such oscillation affects the FD simulation result and the heat flux, leading to unexpected instability. To avoid the large oscillation of this temperature, the average temperature T_{MD} of these three layers every 40 ps ($t - 40$ ps to t) at time point t is used for the right boundary temperature of Domain II. At each time step, the heat flux q'' at the interface is calculated at the right boundary (dark red region in Fig. 1) of Domain II using the FD method. To simulate the cooling effect caused by heat conduction, this heat flux is used to take away energy from the atoms in the left three layers of Domain I (dark red region in Fig. 1) at each simulation step.

The thickness of Domain I is chosen to be greater than the melting depth. Additionally, this thickness is several times the optical absorption depth of the laser. This thickness guarantees that the material in Domain II has negligible laser absorption and have no phase change, that is, only experience heat transfer. The thickness of Domain II is much longer than the thermal diffusion length during the computational time in this work. This assures that the temperature of Domain II bottom (left end) is constant (at 300 K) during the heating and cooling process. In our study, two types of Domain I with different sizes are used. A small Domain I with a size of $1.629 \times 1.629 \times 21.72\,\text{nm}^3$ ($x \times y \times z$) with 2,880 atoms is used for studying surface melting and solidification (§3.1) and critical laser fluence for amorphization (§3.2). A large Domain I of size $1.629 \times 1.629 \times 86.88\,\text{nm}^3$ ($x \times y \times z$) with 11,520 atoms is used for the effect of laser fluence on the amorphous layer thickness (§3.3) and the recrystallization of the amorphous layer (§3.3) simulation. The size of Domain II is $1.629 \times 1.629 \times 12{,}591.304\,\text{nm}^3$ ($x \times y \times z$) which is large enough to capture the heat conduction in the z-direction.

2.2 *Laser absorption in the material*

The wavelength of the laser pulses used in our simulation is 248 nm. This represents a KrF excimer laser in real experiments. The pulse duration of the laser pulse varies from 50 ps to 4 ns. The pulses used for simulation have a uniform spatial energy distribution in the x–y plane (in Fig. 1) and a temporal Gaussian distribution,

$$I(t) = I_0 e^{-(t-t_0)^2/t_g^2}, \tag{1}$$

where $I_0 = E/(t_g \times \pi^{1/2})$, I is the laser intensity, E the pulse energy, t_g is equal to $0.6 \times \text{FWHM}$ (full width at half maximum), t_0 is the peak time of the laser pulse.

In crystalline Si (c-Si), the laser is absorbed exponentially with an optical absorption depth (τ) of 5.54 nm following the formula of $dI/dz = I/\tau$ using the coordinate shown in Fig. 1.[20] Figure 1 also illustrates how the laser beam absorption is treated in the MD domain. Domain I is divided into many layers whose thickness Δz is a little larger than the cutoff distance used in force calculation. Within each time step Δt, the laser energy is absorbed layer by layer. The laser energy absorbed by each layer in Domain I (Fig. 1) is

$$\Delta E = I(z,t) \times (1 - e^{-\Delta z/\tau_z}) \times \Delta t \times A, \tag{2}$$

where A is the cross section of each layer, and $\tau_z = \tau \times \rho_0/\rho_z$ is the local absorption depth of the laser beam, calculated by adjusting τ with the density of ideal c-Si ρ_0 and the local density of Si atoms ρ_z in each layer.[20,21]

Laser beam absorption in each layer in Domain I is achieved by exciting the kinetic energy of atoms, which is fulfilled by scaling the velocities of atoms with an appropriate factor:

$$f = \sqrt{1 + \Delta E/E_{\text{total}}}. \tag{3}$$

Here E_{total} is the total kinetic energy of atoms within each layer. It needs to be pointed out when scaling the velocity of

atoms, only the random movement is scaled while the total momentum is conserved. Details of this laser beam absorption model can be found in our previous work.[21,22)]

2.3 *Procedure of MD and FD simulation*

The time step chosen for the MD and FD simulation is 2 fs. During the simulation, the initial equilibrium temperature of the system is uniform and set to room temperature (300 K). The program takes 500 ps to adjust the system to 300 K. The following 40 ps are used to equilibrate the system and calculate the first average temperature of the three bottom layers (dark red region in Domain I). Then laser heating and heat conduction begin, which are calculated by MD and FD simulations simultaneously. The heating time is set to $2t_0$ for different laser pulses, which is large enough to cover the whole laser pulse. After the laser heating process finishes, the MD simulation for the sample and FD simulation for the substrate continue for a sufficiently long time to simulate the cooling process driven by heat conduction.

3. Results and Discussion

3.1 *Melting and solidification*

As the results of simulations using large Domain I (detailed in §2.2) and high laser fluences, Fig. 2 provides general pictures of the melting and solidification process with amorphization caused by pulsed laser heating and natural heat conduction. In Fig. 2, snapshots of the Si film (Domain I in Fig. 1) at different times illustrate its structural change during the laser heating and natural cooling process. Heated by a laser pulse with $t_g = 4$ ns and fluence of 1300 J/m^2 from 0 to 16 ns ($4t_g$), the Si surface (Domain I in Fig. 1) melts after 6 ns and the top layer of Domain I reaches the boiling point at about 10 ns when the top layer begins to vaporize. The vaporization process ends and Domain I begins to solidify/recrystallize after 14 ns. The solidification concludes at around 22 ns leaving a 12-nm-thick amorphous layer on the top of Domain I.

To characterize the amorphous structure and distinguish it from solid and liquid structures, criteria have to be established to distinguish the amorphous, liquid and crystal Si. In MD simulation, one of the parameters describing the structure characteristics of the crystal, liquid and a-Si is the radial distribution function $g(r)$.[22)] It is a ratio of the number of atoms at a distance r from a given atom compared with the average atom number density in ideal c-Si. The radial distribution function $g(r)$ is calculated for these three structures of Si and is shown in Fig. 3. From Fig. 3, structures of different phases can be quantified. It is shown that the $g(r)$ of c-Si has periodic peaks which reflect the long-range periodicity of ideal crystal. Although a-Si has a much lower temperature than liquid Si, they have similar structures [similar $g(r)$ shown in Fig. 3]. This is because both the liquid and a-Si have similar long-range disordering and short-range ordering structures. It is shown in Fig. 3 that the $g(r)$ of a-Si has higher peaks than the $g(r)$ of liquid Si, which means a less short-range disordering in structure. The $g(r)$ of a-Si also has a significant second peak (the peak at $r/a = 0.7$ in Fig. 3) compared with that of liquid Si. This demonstrates that liquid Si has a more disordering structure than a-Si.

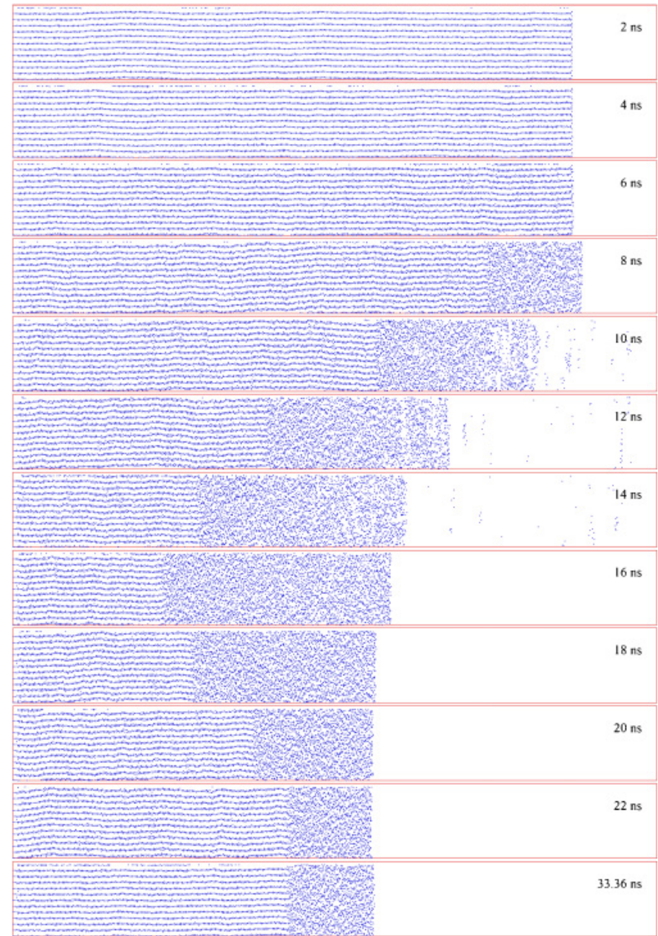

Fig. 2. (Color online) Snapshots of atomic positions in a z–x plane of Domain I for laser amorphization of Si (horizontal: z coordinate, 0–100 nm, vertical: x coordinate, 0–1.7 nm). The laser fluence is 1300 J/m^2, $t_g = 4$ ns. Size of Domain I: $1.629 \times 1.629 \times 86.88$ nm^3 ($x \times y \times z$).

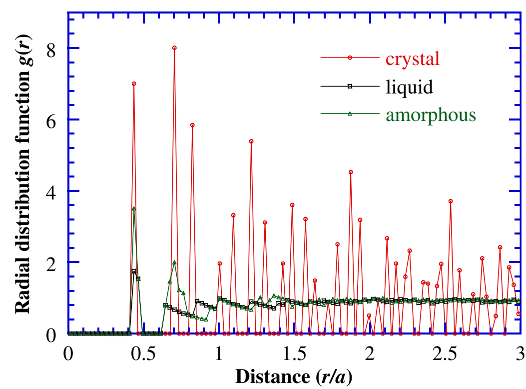

Fig. 3. (Color online) The radial distribution function of crystal, liquid and amorphous structure of Domain I irradiated with a laser fluence of 900 J/m^2 and $t_g = 3$ ns (FWHM = 5 ns).

The temperature profile of the material is studied to distinguish the low temperature a-Si structure and high temperature liquid Si structure. Due to the statistic uncertainty of the liquid/solid interface temperature (there are too few atoms at the interface for temperature calculation), the average temperature of Domain I is calculated to investigate its evolution. Figure 4 gives the temperature evolution of Domain I during the laser amorphization process. The temperature of the top layer reaches the melting point of

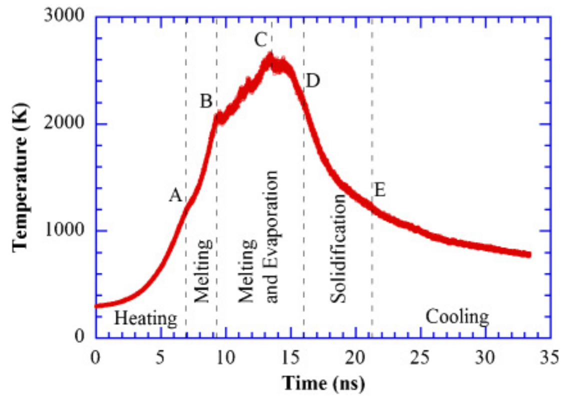

Fig. 4. (Color online) Average temperature evolution of the sample (MD simulation part) during the laser amorphization process ($t_g = 4$ ns, FWHM = 6.67 ns, $E = 300\,\mathrm{J/m^2}$).

c-Si and the surface starts to melt at point A (7 ns, 1200 K). At this time, the average temperature of Domain I is 1200 K, lower than the surface temperature. The surface of Domain I begins to vaporize at point B (9.2 ns, 2050 K) and stops at time point D (16 ns, 2250 K). The latent heat absorption (slope change in Fig. 4) at point A and B indicates the phase change of melting and boiling. The average temperature of Domain I reaches maximum at time point C (13.4 ns, 2600 K), at which the laser pulse energy is equal to the heat conduction energy loss rate. The energy of laser pulse decreases to zero at time point D ($4t_g = 16$ ns) and followed by the solidification process caused by heat conduction. Note that the average temperature at the melting point (point A in Fig. 4) and boiling point (point B in Fig. 4) is less than the experimental values (1687 and 3538 K). That is reasonable because only the top part of material reaches melting and boiling points and begin to melt and boil at point A and C. The temperatures shown in Fig. 4 are the average values of the whole material in Domain I.

Using a smaller size Domain I (detailed in §2.2), melting and solidification processes with and without amorphization are further studied for different laser fluences and pulse widths. The crystal–liquid/amorphous interface is determined using the crystallinity function which has been proved working well in identifying the crystal–liquid interface in our previous work.[23] The physic meaning behind crystallinity function is similar to the X-ray diffraction, but with a much simpler definition of the crystallinity by taking advantage of numerical calculation. This function is designed as

$$\Phi(r_{i,y}) = \frac{1}{N}\left|\sum_i e^{j2\pi(2r_{i,y}/\lambda)}\right|, \qquad (4)$$

where $r_{i,y}$ is the y coordinate of the position of atom i, N the number of atoms within the domain of interest, and λ is the light wavelength. In this work, λ takes the value of a half lattice constant (a). In eq. (4), $2r_{i,y}$ is the distance the light travels when it originates from $y = 0$, reflected by the atom i at the location of $r_{i,y}$, and returns to the original location $y = 0$. If atoms are regularly distributed in space with their spacing in the y direction equal to $n \times a/2$, the function $\Phi(r_{i,y})$ will be equal to 1. In liquid, the function $\Phi(r_{i,y})$ will be much less than 1.

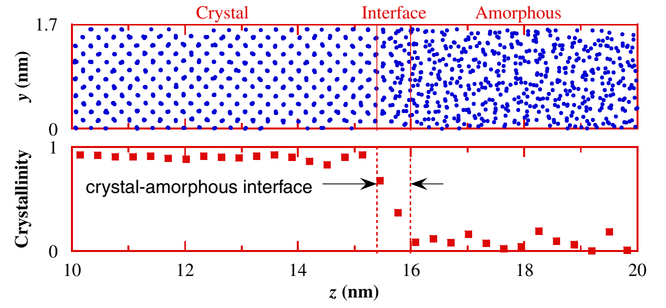

Fig. 5. (Color online) Snapshot of a z–y plane and crystallinity function for crystal, amorphous and crystal–amorphous interface structure. A sharp (~0.7 nm) interface exists between the crystal and amorphous layer.

Figure 5 shows the crystallinity function $\Phi(r_{i,y})$ of the final structure of a Si sample after melting and solidification. It is evident that this function works well in terms of distinguishing the crystal and amorphous regions. In the crystal region, $\Phi(r_{i,y})$ is large, close to 1, showing the sound regularity of the crystal structure. On the other hand, in the amorphous region, randomly distributed atoms in space makes the reflected light have weak diffraction, and $\Phi(r_{i,y})$ becomes very small, between 0 and 0.2.

Using the crystallinity function, Fig. 6 shows the evolution of the crystal–liquid/amorphous interface in the fast melting and solidification process. For laser pulses with the same t_g, the sample recrystallizes to a single crystal perfectly when the laser fluence is smaller than a critical value E_c (detailed in §3.2). Above this value, amorphous layers with different thicknesses are formed on top of the sample. The thickness of the amorphous layer is greater when higher laser fluences being used and when the temperature of the top layer of the sample not reaching the boiling point of Si. Further discussion about the thickness of the amorphous layer and the laser fluence is provided in §3.3. The velocity of the interface movement is around 3–5 m/s. This velocity is less than the critical value (15.8 m/s) measured by transient conductivity experiments.[12–14)]

The mechanism of amorphization by the laser-induced fast cooling originates from the extremely short thermal diffusion length during laser heating. During laser heating, the thermal diffusion depth is limited by the pulse width. The surface region is elevated to a very high temperature in a short time. Therefore, a significant temperature gradient will be established in the surface region (solid part) of Domain I, leading to ultrafast heat conduction to the following cold region (Domain II). Due to the atomic structure difference between the crystal phase and the liquid phase, one having long range periodicity and the other one being aperiodic and amorphous, the transformation between two phases does not happen all of a sudden and consists of two major steps: nucleation (bulk nucleation and epitaxial nucleation) and crystal growth.[24,25] When the cooling rate is extremely high, the liquid does not have enough time to finish the nucleation process, which will result in amorphous phase. From the above mechanism, it is understandable that using a higher laser fluence with a certain FWHM or a shorter FWHM with a certain laser fluence will induce faster melting and a bigger temperature gradient in space, which are more likely to result in amorphous structure.

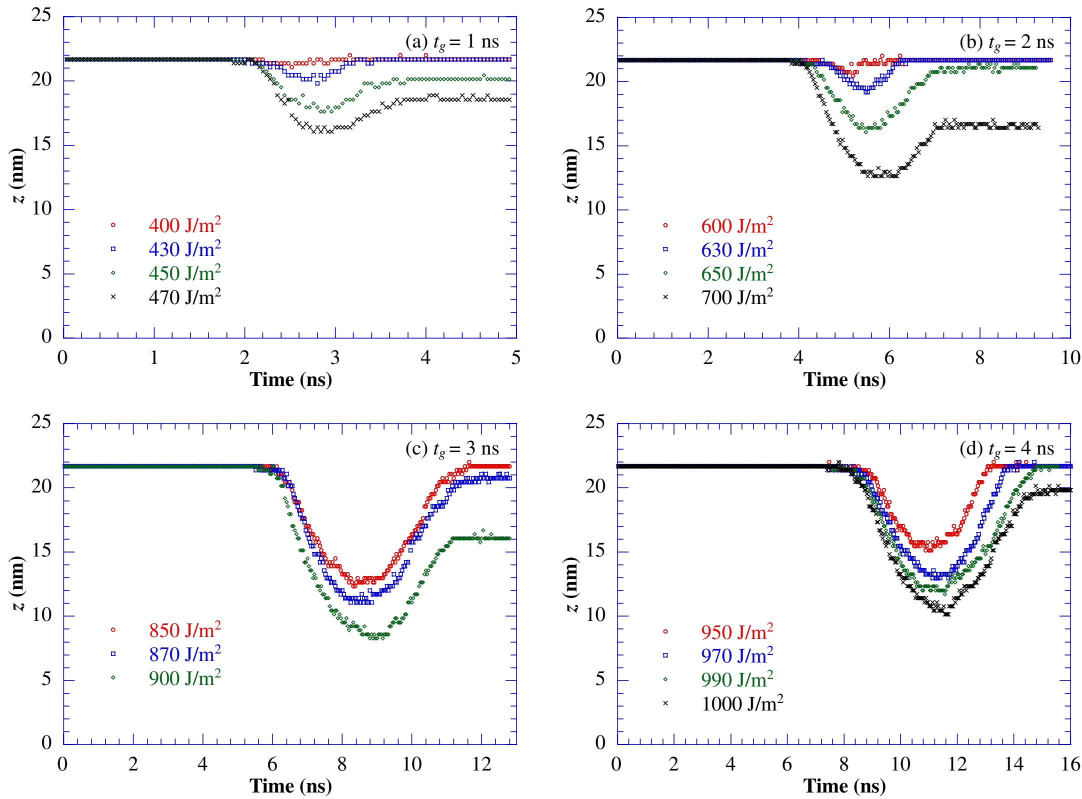

Fig. 6. (Color online) Crystal–liquid/amorphous interface evolution during laser heating and subsequent cooling: (a) $t_g = 1$ ns (FWHM = 1.67 ns), (b) $t_g = 2$ ns (FWHM = 3.33 ns), (c) $t_g = 3$ ns (FWHM = 5 ns), and (d) $t_g = 4$ ns (FWHM = 6.67 ns).

The same conclusions could also be reached from our combined MD-FD simulation results. As shown in Fig. 6, laser pulses with different t_g give the similar results about the relationship between the finial structure and the laser energy. With the same fluence, laser pulses with a smaller t_g results in thicker amorphous layers. It shows that the formation and thickness of the amorphous layer is closely related to the laser properties such as t_g and fluence.

For the amorphous structure formed by pulsed laser-induced ultrafast surface cooling, one important parameter to describe its property is the effective bond order which is defined as $Z_i = \sum_{m \neq i} f(R_{im})$. $f(R_{im})$ is called cutoff function, a measurement of the contribution of a neighboring atom m to atom i in terms of their distance R_{im}.[17] The value of Z reflects the electronic properties of materials. According to work by Justo *et al.*,[17] Z larger than four means metallic bonds among atoms. When Z is less than or equal to four, the atomic bonds tend to be covalent. In this work, the effective bond order Z of c-Si, molten Si and the a-Si layer is calculated. For the case of $t_g = 2$ ns, $E = 700\,\text{J/m}^2$, Z is 4.00, 4.50, and 4.02 for c-Si, molten Si and the amorphous layer, respectively. For the case of $t_g = 3$ ns, $E = 900\,\text{J/m}^2$, Z is 4.00, 4.49, and 4.04 for c-Si, molten Si and the amorphous layer, respectively. In work by Cooper *et al.*,[26] the bond order of a-Si by various numerical simulations and experiments were summarized. Most numerical work reported a bond order larger than four for a-Si while the experimental data is 3.96. This deviation could be attributed to some deficiency in the EDIP used for modeling Si.

3.2 *Critical laser fluence for amorphization*

As discussed in §3.1, amorphization happens when the laser fluence exceeds a certain critical value. In this work, laser pulses with different t_g are used to identify the critical laser fluence above which an amorphous layer will form during post-laser solidification. The t_g takes the range of 0.05–4 ns. Small Domain I is used for simulations in this section. Figure 7 shows the critical fluences of lasers with different FWHMs, which do not exhibit a linear relationship with t_g. Using power function curve fitting, an empirical formula (fitting curve in Fig. 7) is given for the t_g and critical laser fluence:

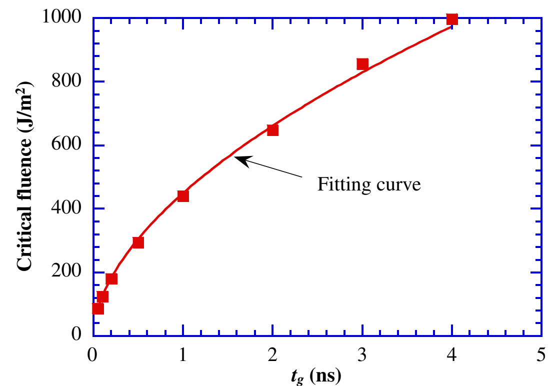

Fig. 7. (Color online) Critical laser fluences with different t_g for amorphization to occur.

$$E_c = 448.76 \times t_g^{0.56}. \tag{5}$$

This relationship could be explained approximately by the heat conduction from the melting region (in Domain I) to the solid part (in Domain II). The formation of the amorphous

layer is induced by the high cooling rate. The critical cooling rate is caused by the critical heat flux between Domains I and II (shown in Fig. 1), which means a unique critical heat flux does exist above which the epitaxial re-growth cannot be sustained. Consider the heat conduction from Domain I to the layer at the thermal diffusion length position of Domain II (at room temperature). The thickness of Domain I could be neglected for the thermal diffusion length (Δl) is much longer than it. Noting that the temperature difference is caused by critical laser fluence (E_c) when the heating laser induces the critical heat flux and neglecting the temperature change caused by heat conduction during the fast laser heating, the critical heat flux (q''_c) is

$$q''_c \propto \frac{T - T_{room}}{\Delta l} \propto \frac{E_c}{\Delta l}, \quad (6)$$

where T is the average temperature of Domain I at the time of laser pulse stops. In our simulation, we find that superheating happens and T is proportional to the overall laser energy input, which leads to eq. (6). From eq. (6) E_c can be estimated as

$$E_c \propto q''_c \times \Delta l \propto q''_c \times (t_g \times \alpha)^{1/2} \propto t_g{}^{1/2}, \quad (7)$$

where α is the thermal diffusivity of Si in Domain I. This first order estimation is very close to the formula concluded from the simulation results.

The structural evolution for (110) Si heated by laser pulses with $t_g = 2$ ns, fluence range of 630–870 J/m^2 and $t_g = 3$ ns, fluence range of 850–900 J/m^2 is also explored in our study. The size of Domain I used for these simulation is $1.536 \times 1.629 \times 21.886$ nm^3 ($x \times y \times z$) with 2,736 atoms. Periodical boundary conditions are applied in the x- and y-directions and free boundary conditions in the z-direction. Domain I with different x–y section sizes is also simulated to validate that the x and y length with periodical boundary condition has little effect on the simulation results. It is shown that the (100) and (110) surface of Si have almost the same melting and solidification velocity. The resulting thicknesses of amorphous layers are also very close for most laser pulses. When the laser fluence is relatively high as 900 J/m^2 ($t_g = 3$ ns), the (110) Si has a little thinner amorphous layer than the (100) Si. The critical laser fluence for both orientation surfaces are found around 650 J/m^2 for $t_g = 2$ ns and 860 J/m^2 for $t_g = 3$ ns. These results indicate that the (100) Si and (110) Si have very close crystallization characteristics and critical laser fluence during ultrafast pulsed laser heating and cooling process.

3.3 *Effect of laser fluence on the amorphous layer thickness*

As discussed in §3.1, the laser fluence is one of the factors affecting the thickness of the amorphous layer besides FWHM. It is shown in Fig. 6 that the thickness of the amorphous layer is proportional to the laser fluence when it exceeds E_c but not too high to cause the top of Domain I to reach the boiling point. The thickness of the amorphous layer created by the laser pulse is usually several nanometers. To achieve a thicker amorphous layer, e.g., 10 nm, high laser fluences are needed. But this may make the situation complicated because high laser fluences may make

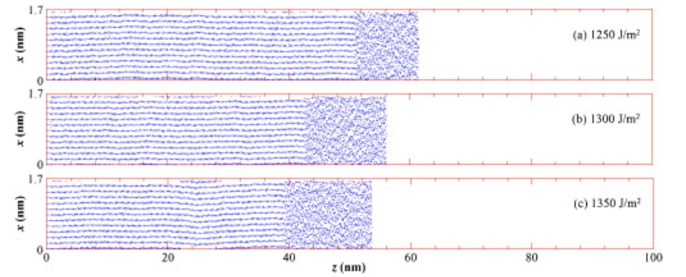

Fig. 8. (Color online) Final structures of the sample for laser amorphization process ($t_g = 4$ ns). The laser fluences are (a) 1250, (b) 1300, and (c) 1350 J/m^2.

Domain I (Si surface) become shorter than its initial thickness by vaporizing its top part. In this section, large Domain I and laser pulses with $t_g = 4$ ns (FWHM = 6.67 ns) are used to study the amorphous layer thickness controlled by the laser fluence when the fluence is large enough to cause the Domain I to experience evaporation (as shown in Fig. 2).

With $t_g = 4$ ns, laser pulses with different fluences result in different amorphous layer thickness. Figure 8 shows the final structure of Domain I after amorphization. When increasing the laser fluence, the sample becomes shorter after solidification because more atoms reach the boiling point of Si and vaporize. Another reason is that a-Si has a higher density than c-Si. Therefore, when the laser fluence is higher, the amorphous layer is thicker, and the overall thickness of the sample looks shorter. When the laser fluence varies from 1250 to 1350 J/m^2, the resulting thicknesses of amorphous layer changes from 10 to 14.5 nm.

3.4 *Recrystallization of the amorphous layer by a second laser pulse*

It is reported that the melting point of a-Si is 200–600 K lower than that of c-Si.[27,28] When heated by a second laser pulse of low/moderate fluence, the amorphous layer melts and recrystallizes to crystal structure for the low laser pulse provides a small heating and cooling rate. Figure 9 shows the crystal–liquid/amorphous interface and temperature evolution of the sample with a 12-nm-thick amorphous layer created by 1300 J/m^2 laser ($t_g = 4$ ns, discussed in §3.1, Fig. 2). Heated by a laser pulse of 900 J/m^2 ($t_g = 4$ ns,

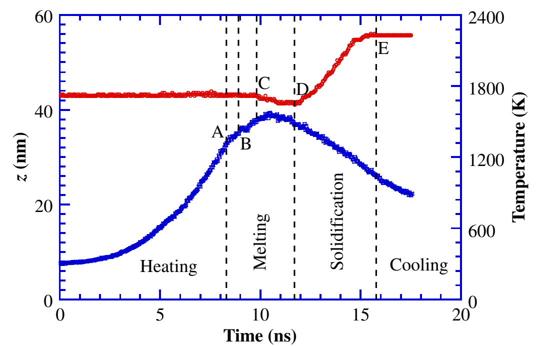

Fig. 9. (Color online) Crystal–liquid/amorphous interface and average temperature evolution of the sample during recrystallization of the amorphous layer by a second laser pulse. $t_g = 4$ ns (FWHM = 6.67 ns), $E = 900$ J/m^2, red line: position of the solid–liquid/amorphous interface; blue line: average temperature of Domain I.

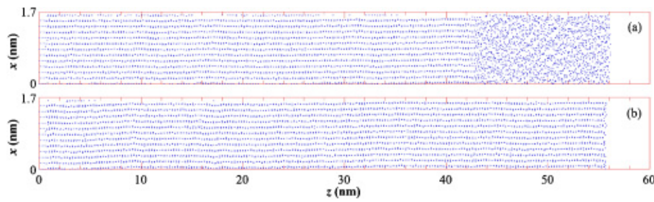

Fig. 10. (Color online) Snapshots of atomic positions: (a) before laser recrystallization (0 ns); (b) after laser recrystallization (17 ns) ($t_g = 4$ ns, FWHM = 6.67 ns).

pulse width is $4t_g$), the amorphous layer begins to melt at point A and the crystal domain begins to melt at time point C. The heating process between time point B (8.9 ns) and C (9.8 ns) heats the following crystal domain to the melting point of c-Si. After point D (11.5 ns), the solidification process begins, and finally the sample recrystallizes to a single crystal at time point E (15.8 ns). Figure 10 shows the snapshots of atomic positions of the sample before and after laser recrystallization using pulsed laser with $t_g = 4$ ns and 900 J/m^2 in fluence. It is shown in Fig. 10 that the amorphous layer crystallizes to crystal structure with a low energy laser pulse. The crystallinity function of the whole crystal part shown in Figs. 10(a) and 10(b) is also calculated and is 0.91 for (a) and 0.90 for (b). These values also prove the final crystal structure after the recrystallization process.

In this work, the amorphization and solidification/crystallization process is for bulk Si subjected to pulsed laser heating, which could quickly melt and amorphize a thin Si layer on the top. Such process has the great potential for formation of ultrathin a-Si layers in the fabrication of metal-on-silicon field-effect transistors. In engineering applications, nanoscale thick Si layers on quartz are also widely seen in processes such as fabrication of photonic band gap crystals using laser-assisted nanoimprinting. In our laboratory, large-scale hybrid atomistic-macroscale simulation is being conducted to study solidification/crystallization of nanometer thick a-Si on quartz. Our preliminary result reveals that the crystallization process is strongly affected by the lattice mismatch between quartz and Si. The lateral size and thickness of the a-Si layer strongly influence the probability and quality of crystallization.

4. Conclusions

With the combined MD/FD simulation, the structural evolution of Si surface heated by pulsed lasers was studied to explore how and to what extent the laser fluence and pulse width affect the amorphization process. It is found that the critical fluence (E_c) for amorphization satisfies a power function relationship with the laser pulse width t_g as $E_c = 448.76 \times t_g^{0.56}$. Such relationship can be explained by the laser-induced strong heat conduction from the molten region to the solid part of the material. Our atomistic study of the amorphous layer structure revealed a sharp interface between the amorphous layer and the crystalline material, and an interface of about 0.6 nm thickness existed between them. The laser fluence was found to have strong effect on the thickness of the amorphous layer. By increasing the fluence of a $t_g = 4$ ns laser pulse from 1250 to 1350 J/m^2, the thickness of the amorphous layer increased from 12 to 14.5 nm. Using a lower laser fluence, the amorphous layer could be recrystallized completely.

Acknowledgements

Support for this work from NSF (CMS: 0457471), Nebraska Research Initiative, Air Force Office for Scientific Research, and MURI from ONR is gratefully acknowledged.

1) D. E. Carlson and C. R. Wronski: Appl. Phys. Lett. **28** (1976) 671.
2) B. K. Nayak, B. Eaton, J. A. A. Selvan, J. Mcleskey, M. C. Gupta, R. Romero, and G. Ganguly: Appl. Phys. A **80** (2005) 1077.
3) T. Suzuki and S. Adachi: Jpn. J. Appl. Phys. **32** (1993) 4900.
4) J. S. Im and H. J. Kim: Appl. Phys. Lett. **63** (1993) 1969.
5) M. Miyasaka and J. Stoemenos: J. Appl. Phys. **86** (1999) 5556.
6) Y.-C. Wang, J.-M. Shieh, H.-W. Zan, and C.-L. Pan: Opt. Express **15** (2007) 6982.
7) F. Plais, P. Legagneux, C. Reita, O. Huet, F. Petinot, D. Pribat, B. Godard, M. Stehle, and E. Fogarassy: Microelectron. Eng. **28** (1995) 443.
8) S. Y. Chou, C. Keimel, and J. Gu: Nature **417** (2002) 835.
9) T. Sameshima and S. Usui: Appl. Phys. Lett. **59** (1991) 2724.
10) A. G. Cullis, N. G. Chew, H. C. Webber, and D. J. Smith: J. Cryst. Growth **68** (1984) 624.
11) U. Landman, W. D. Luedtke, M. W. Ribarsky, R. N. Barnett, and C. L. Cleveland: Phys. Rev. B **37** (1988) 4637.
12) M. O. Thompson, J. W. Mayer, A. G. Cullis, H. C. Webber, N. G. Chew, J. M. Poate, and D. C. Jacobson: Phys. Rev. Lett. **50** (1983) 896.
13) P. A. Stolk, A. Polman, and W. C. Sinke: Phys. Rev. B **47** (1993) 5.
14) A. Polman, P. A. Stolk, D. J. W. Mous, W. C. Sinke, C. W. T. Bulle-Lieuwma, and D. E. W. Vandenhoudt: J. Appl. Phys. **67** (1990) 4024.
15) S. Munetoh, T. Kuranaga, B. M. Lee, T. Motooka, T. Endo, and T. Warabisako: Jpn. J. Appl. Phys. **45** (2006) 4344.
16) R. Ishihara, P. C. van der Wilt, B. D. van Dijk, A. Burtsev, J. W. Metselaar, and C. I. M. Beenakker: Thin Solid Films **427** (2003) 77.
17) J. F. Justo, M. Z. Bazant, E. Kaxiras, V. V. Bulatov, and S. Yip: Phys. Rev. B **58** (1998) 2539.
18) M. Z. Bazant, E. Kaxiras, and J. F. Justo: Phys. Rev. B **56** (1997) 8542.
19) X. Wang, Z. Huang, T. Wang, Y. W. Tang, and X. C. Zeng: Physica B **403** (2008) 2021.
20) D. R. Lide: *CRC Handbook of Chemistry and Physics* (CRC Press, Boca Raton, FL, 2005) 86th ed., p. 12.
21) X. Wang: J. Phys. D **38** (2005) 1805.
22) X. Wang and X. Xu: J. Heat Transfer **124** (2002) 265.
23) X. Wang and Y. Lu: J. Appl. Phys. **98** (2005) 114304.
24) M. Otooni: *Elements of Rapid Solidification: Fundamentals and Applications* (Springer, Heidelberg, 1998) p. 4.
25) S. Steeb and H. Warlimont: *Proc. 5th Int. Conf. Rapidly Quenched Metals* (North-Holland, Amsterdam, 1985) p. 171.
26) N. C. Cooper, C. M. Goringe, and D. R. McKenzie: Comput. Mater. Sci. **17** (2000) 1.
27) P. Baeri, G. Foti, J. M. Poate, and A. G. Cullis: Phys. Rev. Lett. **45** (1980) 2036.
28) Ya. V. Fattakhov, M. F. Galyautdinov, T. N. L'vova, and I. B. Khaibullin: Tech. Phys. **42** (1997) 1457.